A New Rotor Speed Observer for Stand-Alone Brushless Doubly-Fed Induction Generators

Yi Liu
College of Mechanical and Electrical Engineering
Huanggang Normal University
Huanggang, China
liuyi82@hust.edu.cn

Wei Xu
State Key Laboratory of Advanced Electromagnetic Engineering and Technology
School of Electrical and Electronics Engineering
Huazhong University of Science and Technology
Wuhan, China
weixu@hust.edu.cn

Teng Long
Department of Engineering
University of Cambridge
Cambridge, United Kingdom
TL322@cam.ac.uk

Frede Blaabjerg
Department of Energy Technology
Aalborg University
Aalborg, Denmark
fbl@et.aau.dk

***Abstract*—Brushless doubly-fed induction generator (BDFIG) is a new type of ac induction machine and can be used for both grid-connected and stand-alone power generation. The conventional control methods for the BDFIG almost all rely on the encoder, which brings many limitations in terms of cost, complexity, reliability, and so on. This paper presents a new rotor speed observer (RSO) for the encoderless operation of the stand-alone BDFIG, which is based on a rotor position phase-locked loop (PLL) and a second-order generalized integrator (SOGI) and independent of any other machine parameters except for the pole pairs. Comprehensive experiments are also presented to validate the effectiveness of the proposed RSO.**

Keywords— Brushless doubly-fed induction generator (BDFIG); stand-alone power generation system; rotor speed observer (RSO); second-order generalized integrator (SOGI)

I. INTRODUCTION

The brushless doubly-fed induction generator (BDFIG) is a new type of ac induction machine of which stator contains two sets of separate windings with different pole pairs (so called power winding, PW, and control winding, CW, respectively). As a result, its two stator windings are not coupled directly, but indirectly via a specially designed rotor. The configuration of BDFIG is illustrated in Fig. 1. Compared with the Double-Fed Induction Generator (DFIG), the BDFIG, without electric brushes and slip rings, has the merits of longer work life

can be used for both grid-connected and stand-alone power generation, with broad application prospects in the field of wind power and ship shaft power generation.

The steady-state performance of the stand-alone BDFIG system has been investigated in [2]. A stand-alone ship shaft power generator system based on the BDFIG with a wound rotor has been proposed and applied to the power station of a container vessel [3]-[5]. In this system, the voltage amplitude

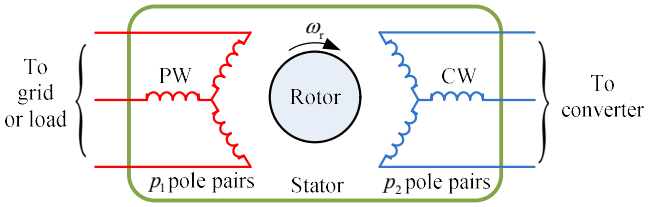

Fig. 1. Configuration of BDFIG.

and frequency of PW are kept constant under variable rotor speeds and loads by utilizing a current vector controller to regulate the CW current. The CW current vector angle, which is the key element of the current vector controller, is derived from the PW voltage reference frequency and the rotor speed. As described in [3]-[5], the rotor speed can be derived from the position of the rotor measured by a shaft encoder. The stator-flux-oriented vector control for the grid-connected BDFIG wind generators has been studied by S. Shao et al. [6], [7], in which the rotor speed is a key element and measured by an encoder. Besides, many other BDFIG research works, almost exclusively rely on the rotor position or speed sensor for closed-loop control, such as phase-angle control [8], indirect stator-quantities control [9], and direct torque control [10].

Nevertheless, the encoderless operation is desirable as shaft encoders bring many drawbacks, such as higher costs and more ty and limited installation order to reduce the cost and complexity of the BDFIG system, and enhance the reliability and application, it is necessary to dynamically observe the rotor speed or position without using shaft encoders.

Some papers have discussed the rotor speed observers (RSOs) for the brushless doubly-fed reluctance generator (BDFRG), which is similar to the BDFIG [11], [12]. It is noted that the RSOs in [11] and [12] both need specific parameters of

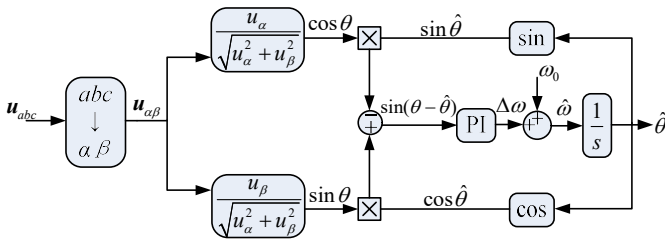

Fig. 2. Structure of the $\alpha\beta$-reference-frame PLL.

the PW inductance and resistance to estimate the flux. However, in the stand-alone BDFIG system in ships, unbalanced and nonlinear loads are frequently connected to the system, leading to distortion of PW voltage and current. Therefore, the PW flux is difficult to accurately estimate, and consequently the observed rotor speed is not accurate. Moreover, the dependence on the machine parameters will also reduce the robustness of the observer.

In order to overcome the above-mentioned problems, a new RSO is proposed in this paper for encoderless operation of the stand-alone BDFIG, which is based on a rotor position phase-locked loop (PLL) and a second-order generalized integrator (SOGI). Such observer is independent to any machine parameters of inductance and resistance although it requires the knowledge of the pole pairs.

This paper is organized as follows: firstly, the fundamentals of BDFIG are described in Section II; and then the principle of the proposed RSO is analyzed in details in Section III; experimental results are given in Section IV; and finally, the conclusions are made in Section V.

II. BDFIG Fundamentals

The BDFM can be operated in several modes, including synchronous, cascade, and induction mode [1]. The synchronous mode, also called the doubly-fed mode, is the optimal one. Under this mode, the rotor speed can be expressed as follows,

$$\omega_r = \frac{\omega_1 + \omega_2}{p_1 + p_2} \tag{1}$$

where p is the pole pairs, and ω is the angular frequency. The subscripts 1, 2, and r represents PW, CW, and rotor, respectively.

When ω_2 is zero, the rotor is rotating at a so-called natural synchronous speed ω_N. Rotor speeds above ω_N are called super-synchronous speeds, and those below ω_N are called sub-synchronous speeds. When the rotor speed varies, in order to keep ω_1 constant, the value of ω_2 should change with the variation of the rotor speed ω_r, and the expression of ω_r can be deduced from (1) as

$$\omega_2 = \omega_r(p_1 + p_2) - \omega_1 \tag{2}$$

III. Design of Rotor Speed Observer for Stand-Alone BDFIGs

A. Rotor Position PLL

The proposed RSO for stand-alone BDFIGs is based on a rotor position PLL (RPPLL). The proposed RPPLL is derived from the $\alpha\beta$-reference-frame PLL [13], [14]. In the $\alpha\beta$-reference-frame PLL as shown in Fig. 2, $\boldsymbol{u}_{abc}$ represents the three-phase voltages, $\boldsymbol{u}_{\alpha\beta}$ the α- and β-components of the voltage vector, θ and $\hat{\theta}$ the actual and estimated phase angles of the voltage vector, and $\hat{\omega}$ and ω_0 are the estimated and nominal angular frequency of the voltage vector. Trigonometric equations are used to calculate the difference $\Delta\theta$ between the actual and estimated phase angles in the vicinity of the equilibrium point, as shown in (3).

$$\Delta\theta = \theta - \hat{\theta} \approx \sin(\theta - \hat{\theta}) = \sin\theta\cos\hat{\theta} - \cos\theta\sin\hat{\theta} \tag{3}$$

The philosophy of the $\alpha\beta$-reference-frame PLL is that the error of the estimated phase angle, $\Delta\theta$, can be controlled to zero by employing a PI controller. The output of the PI controller is the estimated angular frequency $\hat{\omega}$ .The nominal

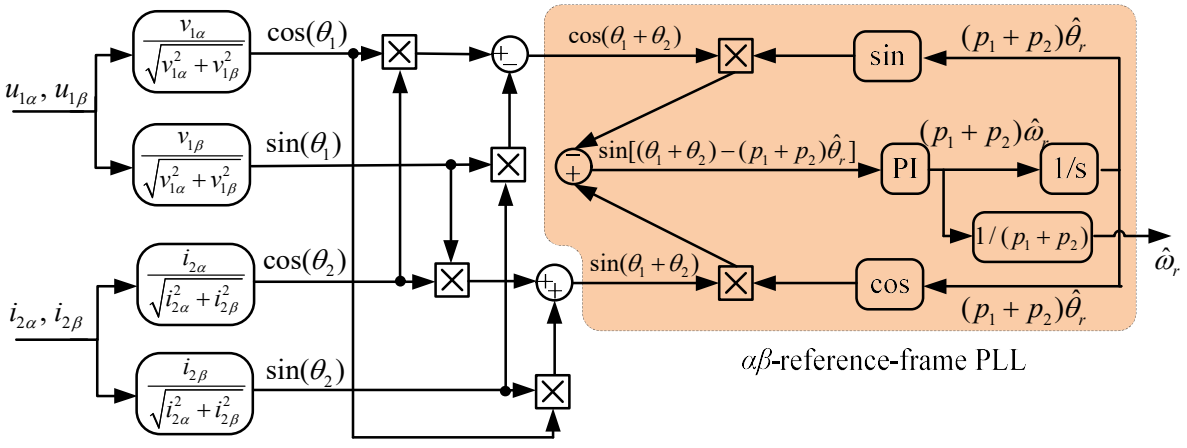

Fig. 3. Block diagram of the rotor position PLL.

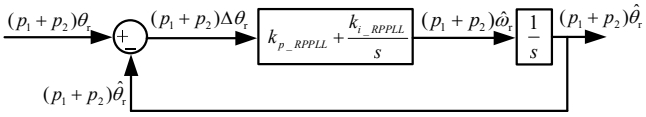

Fig. 4. Linearized control model of the rotor position PLL.

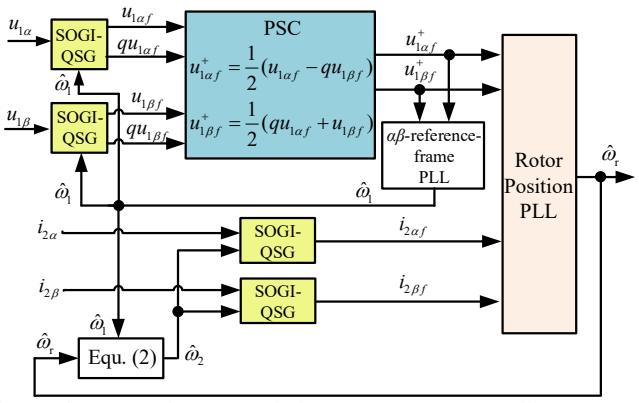

Fig. 5. The proposed rotor speed observer (RSO). PSC: positive-sequence calculator. SOGI-QSG: SOGI-based quadrature-signal generator.

angular frequency ω_0 can be used as a feedforward of the PI controller to improve the dynamic response at startup. The estimated phase angle $\hat{\theta}$ can be obtained by integrating the estimated angular frequency.

Integrating both sides of (1), the following relationship can be derived for the rotor position:

$$(p_1+p_2)\theta_r=\theta_1+\theta_2 \tag{4}$$

where θ_r is the rotor position, θ_1 the PW voltage vector angle, and θ_2 the CW current vector angle.

The proposed RPPLL is illustrated in Fig. 3. The quantities $u_{1\alpha}$ and $u_{1\beta}$ are obtained by the Clark transformation of the three-phase PW voltage, and $i_{2\alpha}$ and $i_{2\beta}$ by the same transformation of the three-phase CW current. The $\sin(\theta_1+\theta_2)$ and $\cos(\theta_1+\theta_2)$ are derived by means of trigonometric calculation and input to the $\alpha\beta$-reference-frame PLL, as shown in Fig. 3. The difference between $(p_1+p_2)\theta_r$ and $(p_1+p_2)\hat{\theta}_r$ can be reduced to zero using a PI regulator, and thus locking the rotor speed and position, having known that in the vicinity of the equilibrium point

$$\begin{aligned}&\sin[(\theta_1+\theta_2)-(p_1+p_2)\hat{\theta}_r]\\&=\sin[(p_1+p_2)\theta_r-(p_1+p_2)\hat{\theta}_r]\approx(p_1+p_2)\Delta\theta_r\end{aligned} \tag{5}$$

Fig. 4 presents the linearized control model of the RPPLL, whose closed-loop transfer function can be expressed as

$$H_\theta(s)=\frac{k_{p\_RPPLL}s+k_{i\_RPPLL}}{s^2+k_{p\_RPPLL}s+k_{i\_RPPLL}} \tag{6}$$

Equation (6) is a second-order transfer function, which can be rewritten to the following standard form

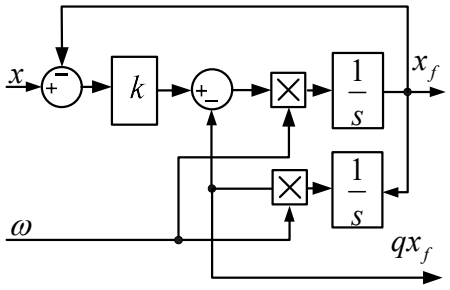

Fig. 6. Structure of the SOGI-QSG.

$$H_\theta(s)=\frac{2\xi\omega_n s+\omega_n^2}{s^2+2\xi\omega_n s+\omega_n^2} \tag{7}$$

Comparing (6) and (7), the following expression can be obtained

$$\omega_n=\sqrt{k_{i\_RPPLL}},\quad \xi=k_{p\_RPPLL}\Big/\left(2\sqrt{k_{i\_RPPLL}}\right) \tag{8}$$

Generally, the damping factor ξ in (7) and (8) is set to be $\sqrt{2}/2$ in order to take into account both the response speed and overshoot of the control system [17]. According to [17], when the reference input is a step signal and the steady-state error is 1%, the settling time t_s of the second-order system shown in (7) can be expressed as

$$t_s=\frac{4.6}{\xi\omega_n} \tag{9}$$

The tuning formula for the PI parameters of the RPPLL can be derived using (8) and (9)

$$k_{p\_RPPLL}=\frac{9.2}{t_s},\quad k_{i\_RPPLL}=\frac{21.16}{(\xi t_s)^2} \tag{10}$$

B. The Proposed Rotor Speed Observer

Generally, the electricity loads of a stand-alone power generation system include both three-phase loads (such as pumps, fans, winders), single-phase loads (such as air conditioners, lighting equipment, communication equipment), and nonlinear loads (such as diode-rectifier, and so on). When the three-phase loads are failed, or the loads of different single-phase power supply lines are not equal, the total load of the stand-alone power generation system becomes unbalanced. The unbalanced load results in an unbalanced PW three-phase current, which produces different voltage drops across the three-phase impedances of the PW, resulting in an unbalanced PW voltage. When the stand-alone power generation system supplies nonlinear loads, the PW voltage will contain significant harmonics. Although the CW is fed by a converter where the voltage is controlled regardless of the distortion of PW voltage, the CW current will have abundant harmonics resulted by the distorted PW voltage due to the indirect coupling via the rotor. The distorted PW voltage and CW current will cause inaccurate rotor speed observation using

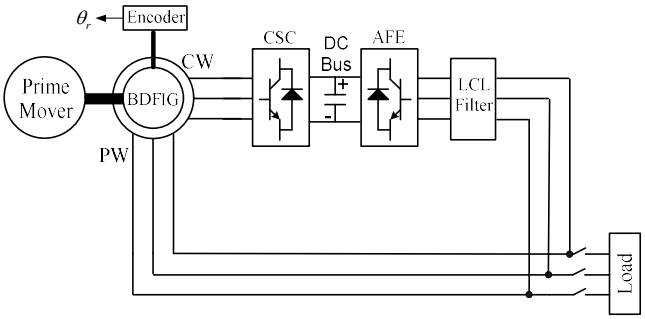

Fig. 7. Structure of the experimental setup. CSC: CW side converter. AFE: active front end.

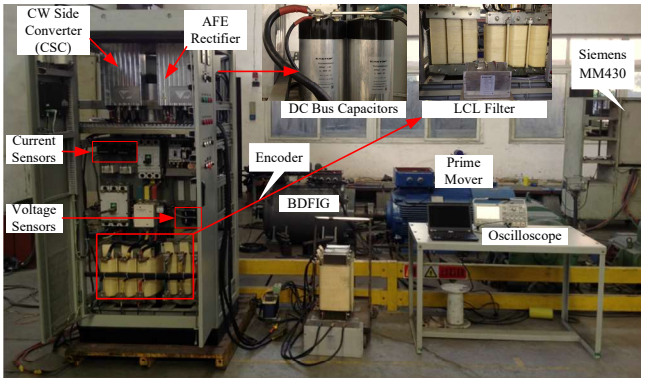

Fig. 8. Photograph of the experimental setup.

only the proposed rotor position PLL.

In order to overcome the aforementioned problems, an SOGI-based quadrature-signal generator (SOGI-QSG) is introduced to construct the RSO for stand-alone BDFIGs as shown in Fig. 5. The structure of the SOGI-QSG is illustrated in Fig. 6, where ω and k are resonance frequency and damping factor of the SOGI-QSG, respectively [15]. The SOGI-QSG is used to obtain the filtered result (x_f) and 90-degree phase shifted version (qx_f) from the input quantity at the same time.

As illustrated in Fig. 5, the quantities $u_{1\alpha f}$, $qu_{1\alpha f}$, $u_{1\beta f}$ and $qu_{1\beta f}$ act as inputs to the positive-sequence calculator (PSC) which lies on the instantaneous symmetrical components (ISC) method on the stationary frame [16]. Then, the positive-sequence $\alpha\beta$ components of the PW voltages are sent to the $\alpha\beta$-reference-frame PLL to make the SOGI-QSGs frequency-adaptive. The two other SOGI-QSGs are employed to adaptively filter the $\alpha\beta$ components of the CW current, where the resonance frequency is derived from (2). Finally, the quantities $u^+_{1\alpha f}$, $u^+_{1\beta f}$, $i_{2\alpha f}$ and $i_{2\beta f}$ are input to the RPPLL to obtain an accurate rotor speed.

IV. Experimental Results

A. Experimental Setup

An experimental setup has been established and it is shown in Fig. 7 and Fig. 8. The experiments are performed on a prototype BDFIG, whose detailed parameters are listed in Table I. A 37 kW three-phase asynchronous motor as the prime mover is mechanically coupled to the BDFIG and driven by a Siemens MM430 inverter. The voltage and current of PW and CW are measured by LEM LV 100 and LEM LT 208-S7/SP1 sensors, respectively. Just for comparison, the actual rotor speed is measured by an incremental encoder (RHI90 from P+F Co.) with a resolution of 1024 cycles/r. The CW side converter (CSC) supplies the CW with frequency-variable exciting current. The active front end (AFE) rectifier with a LCL filter is connected with the PW to regulate the DC bus voltage and achieve bidirectional power flow of the CW.

TABLE I
MAIN PARAMETERS OF PROTOTYPE BDFIG

Parameter	Value
Capacity	30 kVA
Speed range	600 ~1200 rpm
PW pole pairs	1
CW pole pairs	3
PW rated voltage	380 V
PW rated current	45 A
CW voltage range	0~350 V
CW current range	0~40 A
PW resistance	0.4034 Ω
CW resistance	0.2680 Ω
Rotor resistance	0.3339 Ω
PW self-inductance	0.4749 H
CW self-inductance	0.03216 H
Rotor self-inductance	0.2252 H
Mutual inductance between PW and rotor	0.3069 H
Mutual inductance between CW and rotor	0.02584 H
Rotor type	Wound rotor

To give consideration to both the response speed and the stability of the observation system, the settling time t_s and damping factor ξ of the RPPLL is set to be 40 ms and 0.707, respectively. And then, the PI parameters of the RPPLL can be obtained by using (10): $k_{p\_RPPLL} = 230$, $k_{i\_RPPLL} = 26458$. The damping factor of the SOGI-QSG in the RSO is set as 1.414. The tuning method of the PI parameters of the $\alpha\beta$-reference-frame PLL is similar with that of the RPPLL. In these experiments, the settling time and damping factor of the $\alpha\beta$-reference-frame PLL is set to be 30 ms and 0.707, so the proportional and integral coefficients are set to be 306 and 47036, respectively.

B. Results and Analysis

In this part, three typical experiments have been completed. The controller of the experimental machine still uses the encoder to measure the rotor speed. The RPPLL and RSO are employed to observe the rotor speed, respectively. However, the observed results are not fed back to the controller. These experiments are just to compare the performance of the RPPLL and RSO and validate whether the RSO is capable of estimating the rotor speed with similar accuracy offered from an encoder or not.

Experiment 1: The stand-alone BDFIG is operated to supply a balanced three-phase inductive load of 18 kVA with a power factor (PF) 0.7. There is no load connected to the system from 0 s to 4.4 s. At 4.4 s, the inductive load is connected to the

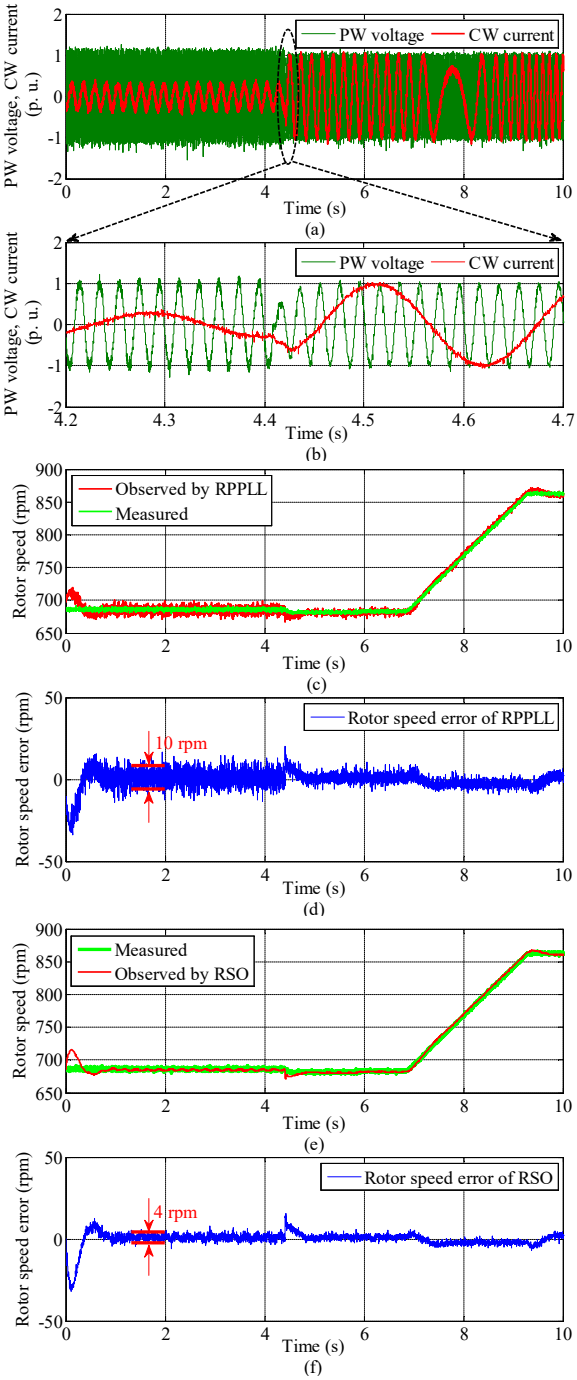

Fig. 9. Results of Experiment 1 for the stand-alone BDFIG supplying a balanced three-phase inductive load of 18 kVA, PF 0.7. (a) PW voltage (1 p. u. = 500 V) and CW current (1 p. u. = 50 A). (b) Detailed view of (a). (c) Rotor speed observed by RPPLL and measured rotor speed. (d) Error of the rotor speed observed by RPPLL. (e) Rotor speed observed by RSO and measured rotor speed. (f) Error of the rotor speed observed by RSO.

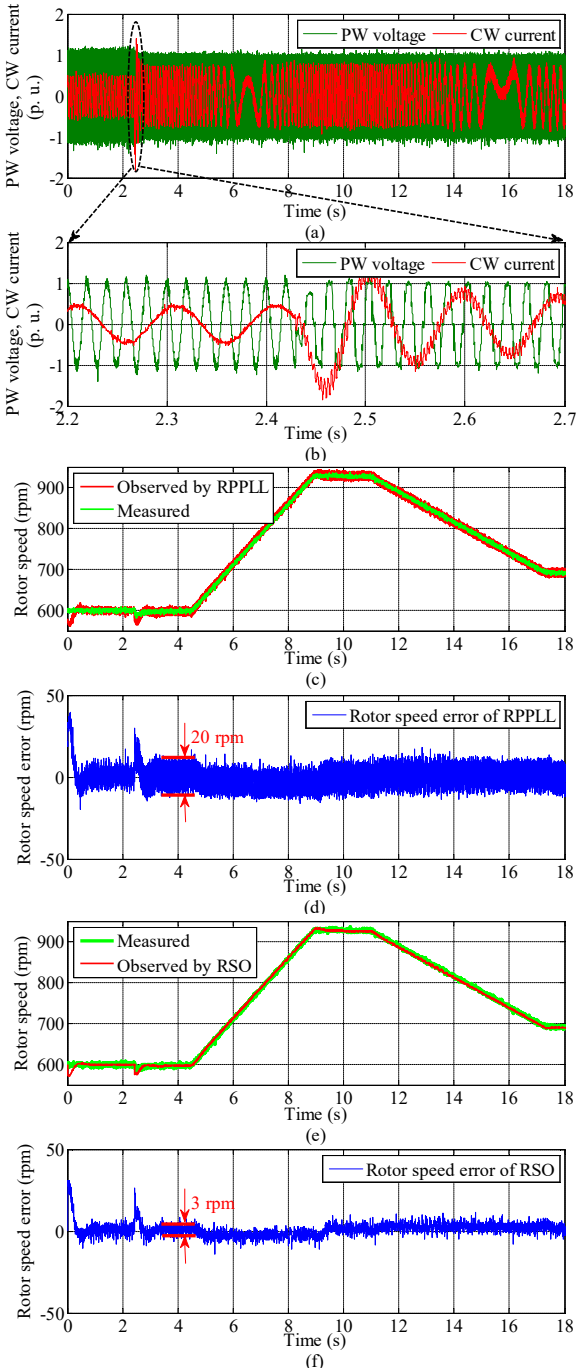

Fig. 10. Results of Experiment 2 for the stand-alone BDFIG supplying a diode-rectifier with a load of 25 Ω resistor. (a) PW voltage (1 p. u. = 500 V) and CW current (1 p. u. = 50 A). (b) Detailed view of (a). (c) Rotor speed observed by RPPLL and measured rotor speed. (d) Error of the rotor speed observed by RPPLL. (e) Rotor speed observed by RSO and measured rotor speed. (f) Error of the rotor speed observed by RSO.

stand-alone BDFIG. Between 6.9 s and 9.3 s, the rotor speed of BDFIG rises from 680 rpm to 860 rpm, with the rapid change of the CW current frequency as shown in Fig. 9(a). The proposed RPPLL and RSO start to operate at 0 s. The rotor speed observed by the RPPLL and the measured rotor speed are shown in Fig. 9(c), and the error between the two rotor speeds is shown in Fig. 9(d). Fig. 9(e) and Fig. 9(f) illustrate the rotor speed observed by the RSO and the corresponding rotor speed error, respectively. When the stand-alone BDFIG runs without loads, the amplitude of the steady-state oscillation

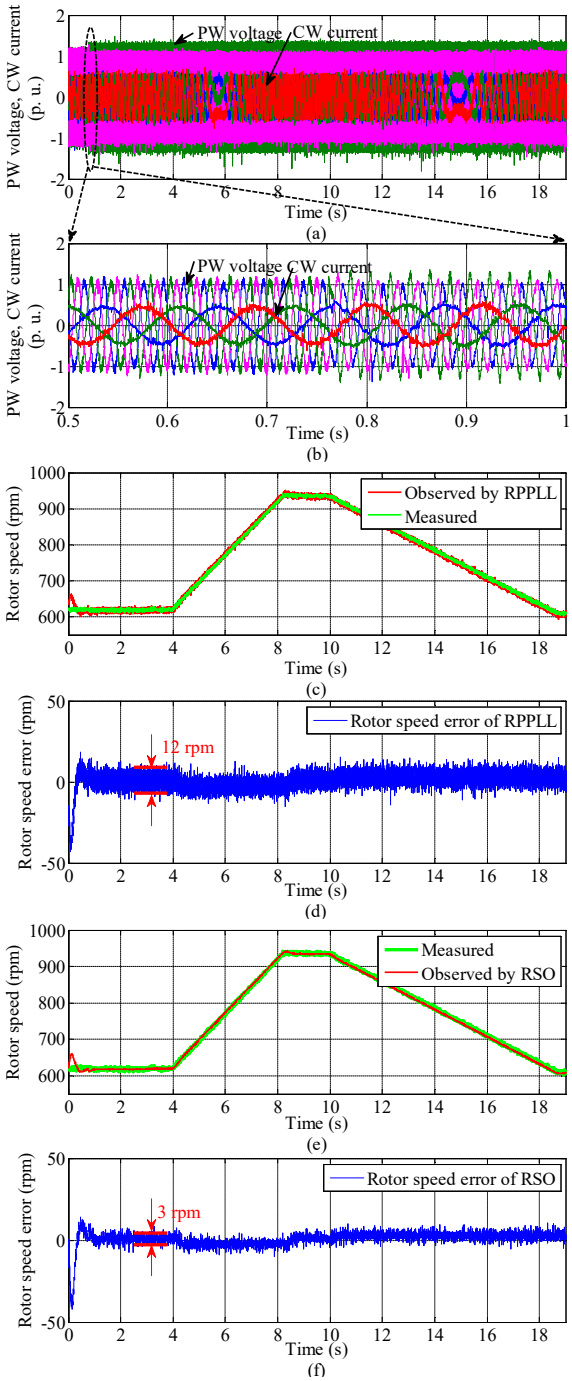

Fig. 11. Results of Experiment 3 for the stand-alone BDFIG supplying an unbalanced three-phase resistive load of 25 Ω, 100 Ω and 100 Ω. (a) PW voltage (1 p. u. = 500 V) and CW current (1 p. u. = 50 A). (b) Detailed view of (a). (c) Rotor speed observed by RPPLL and measured rotor speed. (d) Error of the rotor speed observed by RPPLL. (e) Rotor speed observed by RSO and measured rotor speed. (f) Error of the rotor speed observed by RSO.

in the rotor speed error of the RPPLL is about 10 rpm as shown in Fig. 9(d). However, at the same operation condition, the amplitude of the steady-state oscillation in the rotor speed error of the RSO is significantly reduced to 4 rpm as shown in Fig. 9(f). When the stand-alone BDFIG is connected with the aforementioned inductive load, the steady-state oscillation in the rotor speed error of the RPPLL is similar to that of the RSO. The reason is that the PW voltage harmonics of the stand-alone BDFIG without loads are more than that of the stand-alone BDFIG with loads, and the SOGI in the RSO can adaptively filter the harmonics of the PW voltage. At 4.4 s, the relatively large errors of the rotor speeds observed by the RPPLL and the RSO inevitably come out due to the fluctuations of the PW voltage and CW current caused by the connecting of the inductive load as shown in Fig. 9(b). However, the satisfactory and similar dynamic performance of the RPPLL and the RSO can be achieved. So, the steady-state performance of the proposed RSO can be improved without reducing the dynamic performance.

Experiment 2: The stand-alone BDFIG is connected with a nonlinear load, diode-rectifier with a 25 Ω resistor at the DC side, at 2.43 s. Between 4.46 s and 17.33 s, the rotor speed of the BDFIG rises from 597 rpm to 928 rpm and then goes down to 694 rpm. As shown in Fig. 10(a) and Fig. 10(b), the nonlinear load results in significant harmonics in the PW voltage and CW current. The proposed RPPLL and RSO are activated at 0 s. Comparing the experimental results as shown in Fig. 10(c) - Fig. 10(f), the dynamic response speed of the two observation methods is very similar. At the time of the load being powered, a little error in the speed estimation, about 3.1% of the actual speed, appears and then rapidly converges within 0.28 s as shown in Fig. 10(d) and Fig. 10(f). In addition, the rotor speed observed by the RPPLL and RSO can quickly track the actual one as shown in Fig. 10(c) and Fig. 10(e). However, the steady-state performance of two methods is different. As shown in Fig. 10(d), the amplitude of the steady-state oscillation in the rotor speed error of the RPPLL is about 20 rpm. At the same operation condition, the amplitude of the steady-state oscillation in the rotor speed error of the RSO can be reduced to about 3 rpm as shown in Fig. 10(f). Hence, the RSO has a better overall performance than the RPPLL when the stand-alone BDFIG supplies nonlinear loads.

Experiment 3: At 0.77s, the stand-alone BDFIG is operated to supply an unbalanced three-phase load, each phase of which is 25 Ω, 100 Ω, and 100 Ω, respectively. Between 4 s and 8.2 s, the rotor speed of the BDFIG rises from 620 rpm to 939 rpm. And then, it goes down from 939 rpm to 606 rpm between 10 s and 18.8 s. As it can be seen from Fig. 11(a) and Fig. 11(b), the unbalanced load causes the PW voltage to be significantly unbalanced, which further distorts the CW current. As shown in Fig. 11(c) and Fig. 11(e), the RPPLL and RSO have similar dynamic performance. However, the steady-state performance of the proposed RSO is better than that of the RPPLL. As shown in Fig. 11(d), the amplitude of the steady-state oscillation in the rotor speed error of the RPPLL is about 12 rpm, and it can be significantly reduced to about 3 rpm by the RSO as shown in Fig. 11(f). Hence, the overall performance of the proposed RSO can be improved under the unbalanced load condition.

The effect of the transient error from the observer on the dynamic performance of the control system needs to be discussed in the future. Besides, the performance of the observer at low speed needs to be paid more attention in the

actual application. However, these issues are not the scope of this paper, and will be the future work.

V. Conclusions

This paper has proposed one new RSO for the stand-alone BDFIG to improve the reliability and reduce the cost and complexity of the control system. The principle of the new RSO has been comprehensively analyzed and validated in experiments with several typical loads, the balanced load, the nonlinear and the unbalanced load. By employing the rotor position PLL and SOGI, the proposed RSO demonstrates excellent dynamic performance and very strong robustness capability independent on the parameter. More experimental verification using the proposed RSO of BDFIG will be executed in the BDFIG ship shaft power generation system.

VI. Acknowledgement

This work has been supported by National Natural Science Foundation of China (NSFC), 51377065.

References

[1] R. A. McMahon, P. C. Roberts, X. Wang, and P. J. Tavner, "Performance of BDFM as generator and motor," *IEE Proc.-Electr. Power Appl.*, vol. 153, no. 2, pp.289-299, Mar. 2006.

[2] Y. Liu, W. Xu, G. Zhi, J. Zhang, "Performance analysis of the stand-alone brushless doubly-fed induction generator by using a new T-type steady-state model," *Journal of Power Electronics*, in press.

[3] Y. Liu, W. Ai, B. Chen, K. Chen, and G. Luo, "Control Design of the Brushless Doubly-Fed Machine for Stand-Alone VSCF Ship Shaft Generator Systems," *Journal of Power Electronics*, vol 16, no. 1, pp.259-267, Jan. 2016.

[4] Y. Liu, W. Ai, B. Chen, and K. Chen, "Control design and experimental verification of the brushless doubly-fed machine for stand-alone power generation applications," *IET Electric Power Applications*, vol. 10, no. 1, pp.25-35, 2016.

[5] Y. Liu, W. Ai, B. Chen, and K. Chen, "Operation control of the brushless doubly-fed machine for stand-alone ship shaft generator systems," in *Proc. IEEE Int. Conf. Ind. Tech*., Seville, Spain, pp. 800-805, Mar. 2015.

[6] S. Shao, E. Abdi, F. Barati, and R. McMahon, "Stator-flux-oriented vector control for brushless doubly-fed induction generator," *IEEE Trans. Ind. Electron.*, vol. 56, no. 10, pp. 4220-4228, Oct. 2009.

[7] T. Logan, J. Warrington, S. Shao, and R. McMahon, "Practical deployment of the Brushless Doubly-Fed Machine in a medium scale wind turbine," in *Proc. Int. Conf. PEDS*, pp. 470-475, Nov. 2009.

[8] S. Shao, E. Abdi, and R. McMahon, "Low-cost variable speed drive based on a brushless doubly-fedmotor and a fractional unidirectional converter," *IEEE Trans. Ind. Electron.*, vol. 59, no. 1, pp. 317-325, Jan. 2012.

[9] A. Zhang, X. Wang, W. Jia, and Y. Ma, "Indirect stator-quantities control for the brushless doubly fed induction machine," *IEEE Trans. Power Electron.*, vol. 29, no. 3, pp. 1392-1401, Mar. 2014.

[10] I. Sarasola, J. Poza, M. A. Rodriguez, and G. Abad, "Direct torque control design and experimental evaluation for the brushless doubly fed machine," *Energy Conversion and Management*, vol. 52, no. 2, pp. 1226-1234, Feb. 2011.

[11] M. G. Jovanović, D. G. Dorrell, "Sensorless control of brushless doubly-fed reluctance machines using an angular velocity observer," in *Proc. Int. Conf. Power Electronics and Drive Systems (PEDS)*, pp.717-724, Nov. 2007.

[12] S. Ademi, M. G. Jovanović, H. Chaal, W. Cao, "A New sensorless speed control scheme for doubly fed reluctance generators," *IEEE Trans. Energy Conversion*, vol. 31, no. 3, pp.993-1001, Mar. 2016.

[13] S.-K. Chung, "Phase-locked loop for grid-connected three-phase power conversion systems," *Proc. Inst. Elect. Eng.—Elect. Power Appl.*, vol. 147, no. 3, pp.213–219, May 2000.

[14] R. Teodorescu and F. Blaabjerg, "Flexible control of small wind turbines with grid failure detection operating in stand-alone and grid-connected mode," *IEEE Trans. Power Electron.*, vol. 19, no. 5, pp. 1323–1332, Sep. 2004.

[15] P. Rodríguez, R. Teodorescu, I. Candela, A.V. Timbus, M. Liserre, and F. Blaabjerg, "New positive-sequence voltage detector for grid synchronization of power converters under faulty grid conditions," in *Proc. 37th Power Electronics Specialists Conference*, Jeju, Korea, pp.692-698, 2006.

[16] S. Shao, T. Long, E. Abdi and R. A. McMahon, "Dynamic control of the brushless doubly fed induction generator under unbalanced operation, " *IEEE Trans. on Ind. Electron.*, vol. 60, no. 6, pp.2465-2476, June 2013.

[17] G. Ellis, Control System Design Guide, 3rd ed.. USA: Elsevier Academic Press, 2006.